Rare Met.
DOI 10.1007/s12598-013-xxxxxx

RARE METALS
www.editorialmanager.com/rmet

Multi-Core-shell structured $LiFePO_4@Na_3V_2(PO_4)_3@C$ composite for enhanced low-temperature performance of lithium ion batteries

Xingxing Gu*(iD https://orcid.org/0000-0002-5145-7751**), Xiaolei Ren, Xingyan Liu, Youzhou He, Xiaoteng Liu, Tiefeng Liu*(iD** https://orcid.org/ 0000-0002-3995-2776**)**

Received:*** / Revised: *** / Accepted: ***

Abstract In this work, a multi-core-shell structured $LiFePO_4@Na_3V_2(PO_4)_3@C$ (LFP@NVP@C) composite is successfully designed and prepared to address inferior low-temperature performance of $LiFePO_4$ cathode for lithium ion batteries. TEM confirms the inner NVP and outer carbon layers co-existed on the surface of LFP particle. When evaluated at low-temperature operation, LFP@NVP@C composite exhibits an evidently enhanced electrochemical performance in term of higher capacity and lower polarization, compared with LFP@C. Even at -10 °C with 0.5 *C*, LFP@NVP@C delivers a discharge capacity of *ca*. 96.9 $mAh \cdot g^{-1}$ and discharge voltage of *ca.* 3.3 V, which is attributed to the beneficial contribution of NVP coating. NASICON-structured NVP with an open framework for readily insertion/desertion of Li^+ will effectively reduce the polarization for the electrochemical reactions of the designed LFP@NVP@C composite.

Keywords $LiFePO_4@Na_3V_2(PO_4)_3@C$ composite, Multi-Core-shell, low-temperature, lithium ion batteries

X.-X. Gu*, X.-L. Ren, X.-Y. Liu, Y.-Z. He, Chongqing Key Laboratory of Catalysis and New Environmental Materials, College of Environment and Resources, Chongqing Technology and Business University, Chongqing 400067, China
e-mail: x.gu@ctbu.edu.cn

X.-X. Gu*, X.-T. Liu, Faculty of Engineering and Environment, Northumbria University, Newcastle Upon Tyne, NE1 8ST, UK
e-mail: xingxing.gu@northumbria.ac.uk

T.-F. Liu*
College of Materials Science and Engineering, Zhejiang University of Technology, Hangzhou, 310014, China
e-mail: tiefengliu@zjut.edu.cn

1 Introduction

$LiFePO_4$ (LFP) has been receiving much attention as alternative cathode material for lithium ion batteries (LIBs) due to its excellent thermal safety, environmental friendliness, and abundant sources for low cost[1-3]. Although LFP suffers from intrinsically low electronic and ionic conduction, intensively studies and modifications during recent two decades have enabled a satisfactory rate capability at ambient and high temperatures by methods of coating conductive agents, doping alien ions, and tailoring morphology[4-10]. However, in cold climates and high-altitude drones, LIBs are required to work at subzero temperature. Cold temperature causes sluggish diffusion rate and slow reaction kinetics. Therefore, both discharge capacity and output voltage of LFP are substantially dropped[11-13].

Previous researches have shown that inferior low-temperature performance of LFP is attributed to low Li^+ diffusion of electrode materials and high charge-transfer resistance of electrolyte/electrode interface[13, 14]. Most of the approaches to solve this issue are optimizing electrolyte by introducing additives to tune electrolyte/electrode interface for reducing charge-transfer resistance[11, 12, 15]. In contrast with the electrolyte development, insufficient strides have been achieved in electrode materials design for the low-temperature application. Generally, increasing insertion/desertion channels could accelerate the charge/discharge procedure, even at low-temperature surrounding. Previously, the low-temperature performance of LFP was effectively enhanced by coating $Li_3V_2(PO_4)_3$ material that offers three-dimensional (3D) diffusion channels for insertion/desertion of Li^+, in contrast to one-dimensional (1D) diffusion channels of Li^+ for olivine

structured LFP along the *b* axis[16, 17]. Recently, our group has demonstrated the analogous advantages for providing 3D fast Na^+ diffusion channels in NASICON-structured $Na_3V_2(PO_4)_3$ (NVP) crystals, as thus, which is used as an excellent cathode material for all-climate sodium ion batteries systems[18, 19]. Considering the ionic radius of Li^+ is much smaller than that of Na^+ (0.76 Å *vs.* 1.02 Å) [20, 21], it can be expected that Li^+ could also transfer rapidly in the ion-diffusion channels of NVP. Therefore, coating NVP layer as a fast Li^+ diffusion intermediary should be an effective strategy to assistant the insertion/desertion of Li^+ for LFP at low-temperature.

In this work, we design a multi-core-shell structured LFP@NVP@C composite, in which LFP particles are the cores, NVP as the inner layer to improve the interface kinetics and carbon layer as the outer layer to enhance electronic conductivity of the whole composite, as illustrated in Fig. 1. The low-temperature performances of as-prepared electrodes were systematically investigated through electrochemical characterizations. At -10 °C with rate of 0.5 *C*, LFP@NVP@C delivered a discharge capacity of 96.9 $mAh \cdot g^{-1}$, which is higher than LFP@C (80.2 $mAh \cdot g^{-1}$) without the NVP inner layer and mixed LFP@C/NVP@C composite (80.6 $mAh \cdot g^{-1}$). This enhancement is due to the NVP layer with 3D diffusion channels on the surface of LFP, enabling more insertion/desertion of Li^+ into the crystals and reducing charge-transfer resistance at low temperatures. We do believe this work will open an important window for the research of multifunctional materials for application in low-temperature battery systems.

2 Experimental

2.1 Material synthesis

LFP@C and NVP@C composites were synthesized, respectively, according to our previous report[10, 18]. LFP@C was prepared through rheological phase method, combined with high-energy ball milling process and a subsequent carbothermal reduction. NVP@C was prepared through solid-state method, combined with two-step ball-milling and a subsequent carbothermal reduction. In order to synthesize LFP@NVP@C composite, mixture of LFP@C powder and the precursor of NVP@C (95: 5 by weight) was ball milled at 300 rmp for 3h and further subjected to calcination process at 700 °C for 8 h under Ar. For comparison, LFP@C/NVP@C powder was obtained by mixing LFP@C and NVP@C composites (95: 5 by weight).

2.2 Materials characterizations

X-ray diffraction (XRD) patterns of as-prepared materials were collected on a D/max-γB X-ray diffractometer (Rigaku, Japan) using Cu Kα radiation(λ=1.54178). Diffraction angle was scanned from 10° to 60° at the scanning speed of 0.02° s^{-1}. Morphology and microstructure of as-prepared samples were characterized by high resolution transmission electron microscopy (F30). Inductively coupled plasma atomic emission spectrometry (ICP-AES, Perkin Elmer, 300DV) was used to determine the elemental compositions of the prepared samples. X-ray Photoelectron Spectrometer (XPS) incorporating a 165 mm hemispherical electron energy analyser was used to obtain XPS spectra of the samples. Carbon element was analyzed using vario EL cube (Elementar, Germany).

2.3 Electrochemical measurements

Electrochemical performances of as-prepared samples were evaluated by using a CR2025 coin-type cell. Active materials (80 wt.%), acetylene black (10 wt.%), and a polyvinylidene fluoride (PVdF) binder (10 wt.%) were dispersed in N-methylpyrrolidone (NMP) solvent to form a homogeneous slurry. The slurry was paste on an Al foil and then dried at 100 °C overnight in a vacuum oven to remove NMP. Working electrode was fabricated by cutting round disks of 14 mm in diameter. Asymmetric coin-type cell was assembled with a Li foil as the counter electrode, a polypropylene micro-porous film (Celgard 2400) as separator, a working electrode and organic $LiPF_6$ electrolyte. Symmetric coin-type cell was assembled with two Li foils (or working electrodes) and organic $LiPF_6$ electrolyte. All coin-type cells were assembled in a glove box filled with Ar atmosphere. Galvanostatic charge–discharge tests were investigated by using Neware Battery Testing System at different rates with a voltage window of 2.5~4.2 V (*vs.* Li^+/Li). Cyclic voltammetry (CV) measurements (2.5~4.2 V, 0.1 $mV \cdot s^{-1}$) were performed on CHI 660E electrochemical workstation.

3 Results and discussion

Generally, LFP is modified with carbon layer for core-shell structure to enhance electronic conductivity of the composite[6, 8, 22]. Here, we intend to further modify the surface of LFP with NVP inner layer for enhancing insertion/desertion of Li^+ through constructing multi-core-shell structure. Microstructure of LFP@C and LFP@NVP@C samples were characterized by TEM in Fig. 2. The LFP@C composite is composed of LFP with a high crystallinity and amorphous carbon coating of 2~3 nm (Fig. 2a). Although core-shell structured LFP@C composite allows a sufficient diffusion of Li^+ in the crystals and

electron transfer *via* outer carbon layer, 1D diffusion channels of LFP along the *b* axis only offer a limited window for insertion/desertion of Li^+. The LFP@NVP@C displayed dual coatings consisted of NVP inner layer and carbon outer layer (Fig. 2b). There are evident boundaries between LFP, NVP and carbon. The thicknesses of NVP and carbon layers are 3~4 nm and 1~2 nm, respectively. High-angle annular dark-field scanning TEM (HAADF-STEM) characterized elemental distribution of Fe, V and Na in LFP@NVP@C, as shown in Figure 2c-2f. Uniform distributions of elemental V and Na in the periphery of elemental Fe were witnessed, indicative of the existence of a thin NVP coating layer. Due to 3D Li^+ diffusion channels of NASICON-structured NVP, which is supposed to be an ionic-conductive intermediary with an highly open framework to introduce Li^+ into the LFP@NVP@C composite.

XRD patterns of LFP@NVP@C and LFP@C samples are given in Fig. 3. All diffraction peaks of LFP@NVP@C and LFP@C are indexed as LFP phase (JCPDS No. 81-1173) with an ordered orthorhombic olivine structure, illustrating that low amount of addition of NVP does not influence crystal structure of LFP phase. No traces of carbon in LFP@NVP@C and LFP@C were detected due to that residual carbon is amorphous[10]. The carbon content of LFP@NVP@C and LFP@C is 1.85 wt.% and 1.35 wt.%, respectively. No diffraction peaks of LFP@NVP@C corresponding to NVP phase were collected due to low amount of NVP component. ICP was further employed to characterize the elemental compositions of LFP@NVP@C and demonstrated that the percentage of V element was *ca.* 1.08 wt.%, which is consistent well with the V weight ratio of raw materials (1.11%). Further structure information about LFP@NVP@C was characterized by X-ray photoelectron spectra (XPS), as shown in Fig. 4. Elemental V was confirmed in LFP@NVP@C. High resolution of C 1s of LFP@NVP@C shows that there is most of sp^2-type carbon, indicating a highly graphitized carbon layer that can facilitate electronic migration[23]. In the high resolution XPS spectrum of V 1s, the peak at binding energy of 515.75 eV belongs to the V(III)[18].

Electrochemical performances of LFP@NVP@C and LFP@C were first investigated galvanostatic charge/discharge tests at various temperatures, as shown in Fig. 5. At the rate of 0.5 *C*, discharge capacities of LFP@NVP@C are 160.9, 111.8, 96.9 and 59.2 $mAh \cdot g^{-1}$ at 23 °C, 0 °C, -10 °C, and -25 °C, respectively, which are 2.2%, 3.6%, 15.5%, and 18.6% higher than that of LFP@C. Compared with LFP@C, LFP@NVP@C delivers lower charge plateaus as well as higher discharge plateaus, indicating a smaller polarization for interfacial reaction between electrolyte and electrode. Even at -25 °C, LFP@NVP@C delivers discharge voltage of *ca.* 3.2 V, respectively, which potentially ensures sufficient power density of LIBs at low temperatures. Coulomb efficiencies of LFP@NVP@C are near 100% at various temperatures. Therefore, LFP@NVP@C exhibits a better electrochemical performance than LFP@C due to the contribution of NVP layer. The NASICON-structured NVP has open framework to offer fast insertion/desertion of Li^+ for LFP@NVP@C.

Rate performances of as-prepared electrodes containing LFP@C/NVP@C were further evaluated at various temperatures, as shown in Fig. 6. At 23 °C, LFP@NVP@C, LFP@C and LFP@C/NVP@C electrodes exhibit similar electrochemical performances at most rates. Room temperature ensures sufficient reaction kinetics for the release of capacity of electrode materials. Only one different for three as-prepared electrodes occurs at the rate of 10 *C*. LFP@NVP@C and LFP@C/NVP@C deliver discharge capacities of *ca.* 100.1 mAh g^{-1} and 93.0 mAh g^{-1}, respectively, which both exceed LFP@C (82.3 mAh g^{-1}), indicating that the addition of NVP into LFP is effective for rate performance. In addition, the discharge capacity of LFP@NVP@C is high than that of LFP@C/NVP@C, illustrating that NVP layer based on multi-core-shell structure plays a beneficial role on facilitating more insertion/desertion of Li^+ into LFP crystal. As temperature decreased, effectiveness of NVP coating on improvement of low-temperature performance becomes more distinct. In contrast to LFP@C suffering from inferior low-temperature performance, LFP@NVP@C exhibits enhanced electrochemical properties of Li^+ storage. At 0 °C, discharge capacities of LFP@NVP@C are 111.8, 97.6, 84.4 and 61.8 $mAh \cdot g^{-1}$ at 0.5, 1, 2, and 5 *C*, respectively, which are 8.3%, 10.4%, 16.1%, and 33.7% higher than that of LFP@C. Interestingly, discharge capacities of LFP@C/NVP@C are side by side with that of LFP@C at less than 5 *C*, while are much close to that of LFP@NVP@C at 10 *C*. The NVP@C has been reported to have an excellent low-temperature performance, and therefore NVP@C make major contribution for discharge capacity of mixed LFP@C/NVP@C electrode[13, 18]. At -10 °C, LFP@NVP@C still delivered discharge capacities of 96.9, 82.2, 66.7 and 41.6 $mAh \cdot g^{-1}$ at 0.5, 1, 2, and 5 *C*, respectively. Even at -25 °C, LFP@NVP@C exhibited the best rate performance among three as-prepared electrodes.

The NVP with 3D framework and multi-core-shell structure leads to an enhanced low-temperature performance of LFP@NVP@C.

To understand the origin of enhanced low-temperature performance of the LFP@NVP@C, electrochemical kinetics of LFP@NVP@C and LFP@C were first evaluated by cyclic voltammetry (CV) technique in Fig. 7. A pair of redox peaks of LFP@C was evidently collected at 23 ºC, corresponding to the Li^+ insertion/de-insertion in LFP crystals in conjunction with two phase charge/discharge reaction of Fe^{2+}/Fe^{3+} redox couple[6, 10, 24]. As operating temperature decreases down to -25 ºC, the potential interval between anodic/cathodic peaks increases from 333 mV to 787 mV and peak current drops to a quarter of room value, which indicates a slowdown of electrochemical reactions of LFP@C. As for LFP@NVP@C, similar to LFP@C, increased polarization and reduced peak current were also observed with decreasing operating temperature. Potential intervals of LFP@NVP@C are 298, 442, 579, and 758 mV at 25, 0, -10, and -25 °C, respectively, which are lower than those of LFP@C, implying that this polarization was relieved by NVP coating layer.

Following we analyze electrochemical impendence spectra (EIS) at various temperatures. As displayed in Fig. 8a and 8b, as operating temperature decreases, the diameters of semicircles in the profiles of LFP@C//Li and LFP@NVP@C//Li half-cell become significantly larger, respectively. Similarly, the EIS curves of symmetric Li//Li cell also exhibit a rapidly increased semicircle diameter and thus increased impedance (Fig. 8c). Such increases are well consistent with our recent previous works that dramatically increased charge-transfer resistances of half-cell at low temperatures are mainly resulted from metallic anode[17, 18, 25], which has demonstrated that using half-cell was not best mode to assess charge-transfer resistance of targeted materials.

Therefore, we further assessed EIS spectrum of LFP@C and LFP@NVP@C with symmetric cells. As shown in Fig. 9a and 9b, symmetric LFP@C//LFP@C and LFP@NVP@C//LFP@NVP@C cells offer a single semicircle with similar diameters (Fig. 9a and 9b), illustrating that the Li electrode is responsible for the increased impedance[18]. In EIS curves of Figure 9a and 9b, the intersection on the *x* axis represents bulk resistance of the cell (R_u) including the electrolyte and electrodes[4], and semicircle diameter represents corresponding charge-transfer resistance (R_{ct}) reflecting electrochemical kinetics of interfacial reaction[17]. All the values of R_u and R_{ct} are listed in Table 1. The R_u values escalate with decreasing temperature, which are mainly ascribed to reduced Li^+ diffusion in the electrolyte[26, 27]. An increase in the values of R_{ct} indicates that decreased operating temperatures make reaction kinetics of electrode difficult. Compared with LFP@C, LFP@NVP@C exhibits lower R_{ct} values from 43.74 to 54.55 with decreasing temperature. The NVP offers easy access to Li^+ for LFP and thus enables LFP@NVP@C more capacity and lower polarizations than LFP@C during the charge/discharge. In addition, the apparent Li^+ diffusion coefficient (D_{Li}) is calculated by the straight slope lines at low frequency region[28, 29]. The Warburg coefficient σ can be calculated by Equation 1.

$$|Z'| = R_s + R_{ct} + \sigma\omega^{-0.5} \quad (\omega \text{ is frequency}) \quad (1)$$

The plot of Z_{im} vs. the reciprocal square root of the low angular frequency is given in Fig. 9c and 9d. The slope of the fitted line is the Warburg coefficient σ. The calculated values of σ for LFP@NVP@C and LFP@C are given in Table 1. Subsequently, because ionic diffusion coefficient (D_{Li}, $cm^2 \cdot s^{-1}$) is inversely proportional to σ, the D_{Li} values can be further calculated by the following Equation 2.

$$D_{Li} = R^2T^2 / 2A^2n^4F^4c^2\sigma^2 \quad (2)$$

where R is the gas constant, T is the absolute temperature (K), A is the apparent area of electrode (cm^2), n is the number of electrons per molecule during the intercalation (n = 1), F is the Faraday constant, c is the Li^+ concentration ($mol \cdot cm^{-3}$) and σ is the Warburg coefficient. Therefore, the calculated D_{Li} values at various temperatures are shown in Table 1.

The variation of the values of D_{Li} is higher for LFP@C than LFP@NVP@C, which is benefited from NVP layer with a stable 3D framework offering sufficient interstitial window to allow fast insertion/desertion of Li^+ into the crystal. The reduced charge-transfer resistance and improved insertion/desertion of Li^+ bring an enhanced low-temperature performance of LFP@NVP@C.

4 Conclusion

We successfully synthesized a multi-core-shell structured LFP@NVP@C composite to enhance low-temperature performance of LIBs. NVP process an open framework for easy insertion/desertion of Li^+ into/ out of the crystal, and the introduction of NVP interlayer is to modify the surface of LFP crystal by offering more diffusion channels of Li^+. As the temperature falls, LFP@NVP@C exhibited an enhanced low-temperature performance by *ca.* 8~33% in comparison with LFP@C, which is attributed to reduced charge-transfer resistance and enhanced Li^+ diffusion. Even at -10 ºC with 0.5 *C*, LFP@NVP@C delivered a discharge capacity of *ca.* 96.9 $mAh \cdot g^{-1}$ and discharge voltage of *ca.* 3.3 V. Our achievements suggest that tuning the surface of cathodes or anodes with materials of multi-dimensional

diffusion channels is an effective method to enhance low-temperature performance of LIBs.

Acknowledgments This work was supported by the National Natural Science Foundation of China (No. 51902036), Natural Science Foundation of Chongqing Science & Technology Commission (No. cstc2019jcyj-msxm1407), and the Engineering and Physical Sciences Research Council (EPSRC) (Grant No. EP/S032886/1).

References

[1] Dimesso L, Forster C, Jaegermann W, Khanderi JP, Tempel H, Popp A, Engstler J, Schneider JJ, Sarapulova A, Mikhailova D, Schmitt LA. Oswald S. and Ehrenberg H., Developments in nanostructured $LiMPO_4$ (M = Fe, Co, Ni, Mn) composites based on three dimensional carbon architecture. Chem Soc Rev 2012; 41: 5068.

[2] Li X, Jiang YZ, Li XK, Jiang HX, Liu JL, Feng J. Electrochemical property of $LiFePO_4$/C composite cathode with different carbon sources. Rare Met 2018; 37: 743.

[3] Zhou JX, Shen XQ, Jing MX, Zhan Y. Synthesis and electrochemical performances of spherical $LiFePO_4$ cathode materials for Li-ion batteries. Rare Met 2006; 25: 19.

[4] Wang B, Abdulla W, Wang D, Zhao XS. A three-dimensional porous $LiFePO_4$ cathode material modified with a nitrogen-doped graphene aerogel for high-power lithium ion batteries. Energy Environ. Sci. 2015; 8: 869.

[5] Wang B, Liu T, Liu A, Liu GJ, Wang L, Gao TT, Wang DL, Zhao XS. A hierarchical porous C@$LiFePO_4$/carbon nanotubes microsphere composite for high-rate lithium-ion batteries: combined experimental and theoretical study. Adv Energy Mater 2016; 6: 1600426.

[6] Xiong QQ, Lou JJ, Teng XJ, Lu XX, Liu SY, Chi HZ, Ji ZG. Controllable synthesis of N-C@$LiFePO_4$ nanospheres as advanced cathode of lithium ion batteries. J Alloys Compd. 2018; 743: 377.

[7] Wang X, Feng Z, Hou X, Liu L, He M, He X, Huang JT, Wen Z. Fluorine doped carbon coating of $LiFePO_4$ as a cathode material for lithium-ion batteries. Chem Eng J 2020; 379: 122371.

[8] Zhang Y, Xin P, Yao Q. Electrochemical performance of $LiFePO_4$/C synthesized by sol-gel method as cathode for aqueous lithium ion batteries. J Alloys Compd 2018; 741: 404.

[9] Busson C, Blin MA, Guichard P, Soudan P, Crosnier O, Guyomard D, Lestriez B. A primed current collector for high performance carbon-coated $LiFePO_4$ electrodes with no carbon additive. J Power Sources 2018; 406: 7-17.

[10] Liu T, Zhao L, Wang D, Zhu J, Wang B, Guo C. Carbon-coated single-crystalline $LiFePO_4$ nanocomposites for high-power Li-ion batteries: the impact of minimization of the precursor particle size. RSC Adv 2014; 4: 10067.

[11] Liao XZ, Ma ZF, Gong Q, He YS, Pei L, Zeng LJ. Low-temperature performance of $LiFePO_4$/C cathode in a quaternary carbonate-based electrolyte. Electrochem Commun 2008; 10: 691.

[12] Liao L, Fang T, Zhou X, Gao Y, Cheng X, Zhang L, Yin, G. Enhancement of low-temperature performance of $LiFePO_4$ electrode by butyl sultone as electrolyte additive. Solid State Ionics 2014; 254: 27.

[13] Liao L, Zuo P, Ma Y, Chen X, An Y, Gao Y, Yin G. Effects of temperature on charge/discharge behaviors of $LiFePO_4$ cathode for Li-ion batteries. Electrochim Acta 2012; 60: 269.

[14] Li C, Hua N, Wang C, Kang X, Tuerdi W, Han Y. Effect of Mn^{2+}-doping in $LiFePO_4$ and the low temperature electrochemical performances. J Alloys Compd 2011; 509: 1897.

[15] Liao L, Cheng X, Ma Y, Zuo P, Fang W, Yin G, Gao Y. Fluoroethylene carbonate as electrolyte additive to improve low temperature performance of $LiFePO_4$ electrode. Electrochimica Acta 2013; 87: 466.

[16] Yang G, Jiang CY, He XM, Ying JR, Gao J. Preparation of $Li_3V_2(PO_4)_3$/$LiFePO_4$ composite cathode material for lithium ion batteries. Ionics 2013; 19: 1247.

[17] Rui XH, Jin Y, Feng XY, Zhang LC, Chen CH. A comparative study on the low-temperature performance of $LiFePO_4$/C and $Li_3V_2(PO_4)_3$/C cathodes for lithium-ion batteries. J Power Sources 2011; 196: 2109.

[18] Liu, T, Wang B, Gu X, Wang L, Ling M, Liu G, Wang D, Zhang, S. All-climate sodium ion batteries based on the NASICON electrode materials. Nano Energy 2016; 30: 756.

[19] Jian Z, Zhao L, Pan H, Hu YS, Li H, Chen W, Chen L. Carbon coated $Na_3V_2(PO_4)_3$ as novel electrode material for sodium ion batteries. Electrochem Commun 2013; 14: 86.

[20] Gaubicher J, Wurm C, Goward G, Masquelier C, Nazar L. Rhombohedral form of $Li_3V_2(PO_4)_3$ as a cathode in Li-ion batteries. Chem Mater 2000; 12:3240.

[21] Jian Z, Han W, Liang Y, Lan Y, Fang Z, Hu YS, Yao Y. Carbon-coated rhombohedral $Li_3V_2(PO_4)_3$ as both cathode and anode materials for lithium-ion batteries: electrochemical performance and lithium storage mechanism. J Mater Chem A 2014; 2: 20231.

[22] Hongtong R, Thanwisai P, Yensano R, Nash J, Srilomsak S, Meethong N. Core-shell electrospun and doped $LiFePO_4$/FeS/C composite fibers for Li-ion batteries. J Alloys Compd 2019; 804: 339.

[23] Wang Y, Alsmeyer DC, McCreery RL. Raman spectroscopy of carbon materials: structural basis of observed spectra. Chem Mater 1990; 2: 557.

[24] Ren L, Li XE, Wang FF, Han Y. Spindle $LiFePO_4$ particles as cathode of lithium-ion batteries synthesized by solvothermal method with glucose as auxiliary reductant, Rare Met 2015; 34: 731.

[25] Iermakova DI, Dugas R, Palacín MR, Ponrouch A. On the comparative stability of Li and Na metal anode interfaces in conventional alkyl carbonate electrolytes. J Electrochem Soc 2015; 162: A7060.

[26] Liao L, Zuo P, Ma Y, An Y, Yin G, Gao Y. Effects of fluoroethylene carbonate on low temperature performance of mesocarbon microbeads anode. Electrochim Acta 2012; 74: 260.

[27] Gu X, Xin L, Li Y, Dong F, Fu M, Hou Y. Highly reversible Li–Se batteries with ultra-lightweight N, S-codoped graphene blocking layer. Nano Micro Lett 2018; 10: 59.

[28] Wang B, Wang Q, Xu B, Liu T, Wang D, Zhao G. The synergy effect on Li storage of $LiFePO_4$ with activated carbon modifications. RSC Adv 2013; 3: 20024.

[29] Gu XX, Yang Z, Qiao S, Shao CB, Ren XL, Yang JJ. Exploiting methylated amino resin as a multifunctional binder for high-performance lithium–sulfur batteries. Rare Met 2020; doi.org/10.1007/s12598-020-01409-1.

Tables

Table 1 The R_u, R_{ct}, σ and D_{Li} of LFP@C and LFP@NVP@C

	LFP@C				LFP@NVP@C			
Temperature / ^oC	23	0	-10	-25	23	0	-10	-25
R_u / Ω	3.89	8.89	16.76	26.57	3.69	9.36	13.09	19.41
R_{ct} / Ω	51.41	70.08	78.36	79.32	43.74	48.32	52.18	54.55
σ / Ω	507.81	1556.53	2060.50	2689.49	490.69	1416.80	1863.61	2421.32
D_{Li} / $\times 10^{-18}$ $cm^2 \cdot s^{-1}$	110	9.96	5.28	2.75	117	12.02	6.449	3.40

RARE METALS
www.editorialmanager.com/rmet

Figures

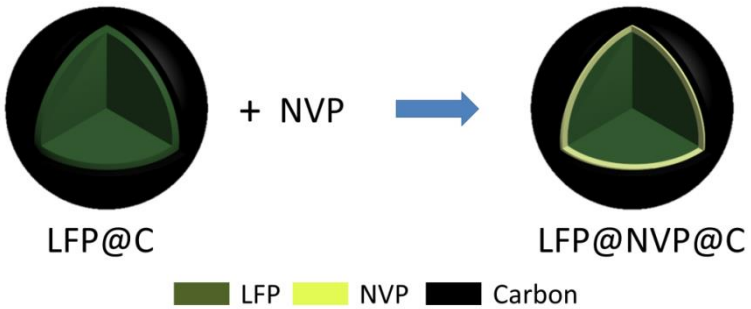

Fig.1 Schematic illustration used to synthesize LFP@NVP@C composite

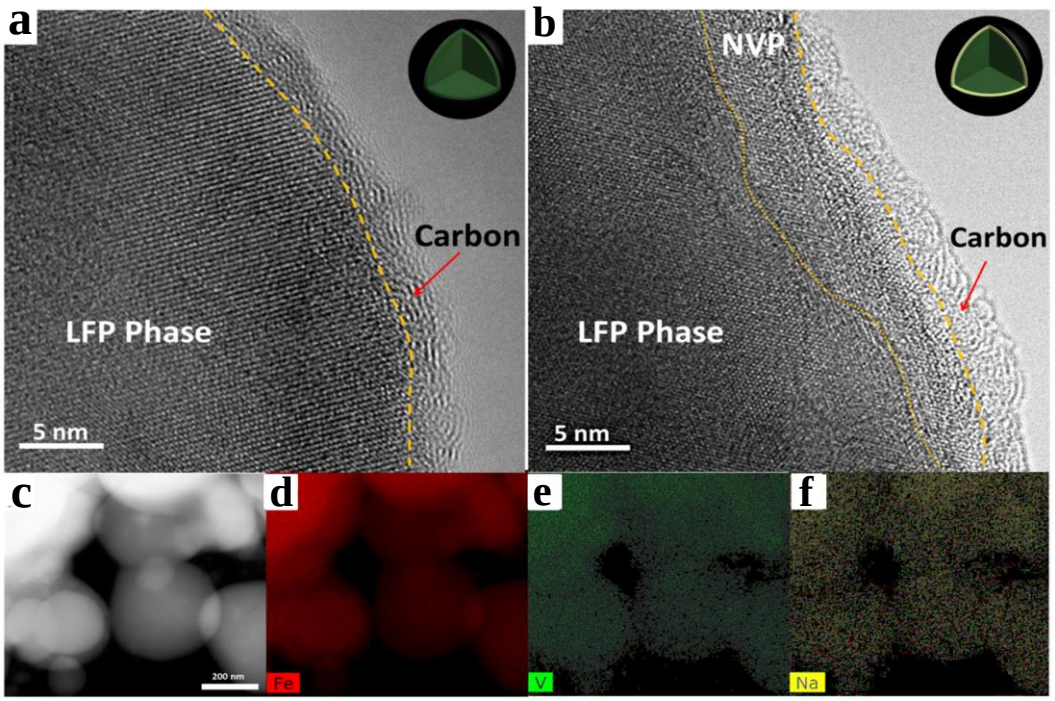

Fig.2 TEM images: (a) LFP@C and (b) LFP@NVP@C. HAADF-STEM for LFP@NVP@C: (c) Position and elemental distribution of (d) Fe, (e) V and (f) Na.

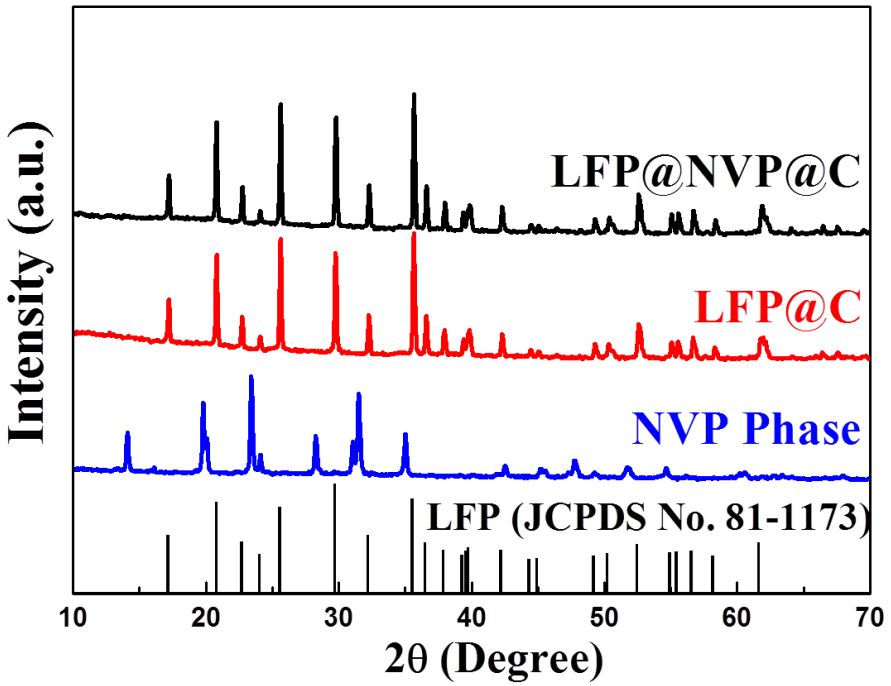

Fig.3 XRD patterns of LFP@NVP@C, LFP@C, NVP[18], and LFP (ICDD PDF No. 40-1499)

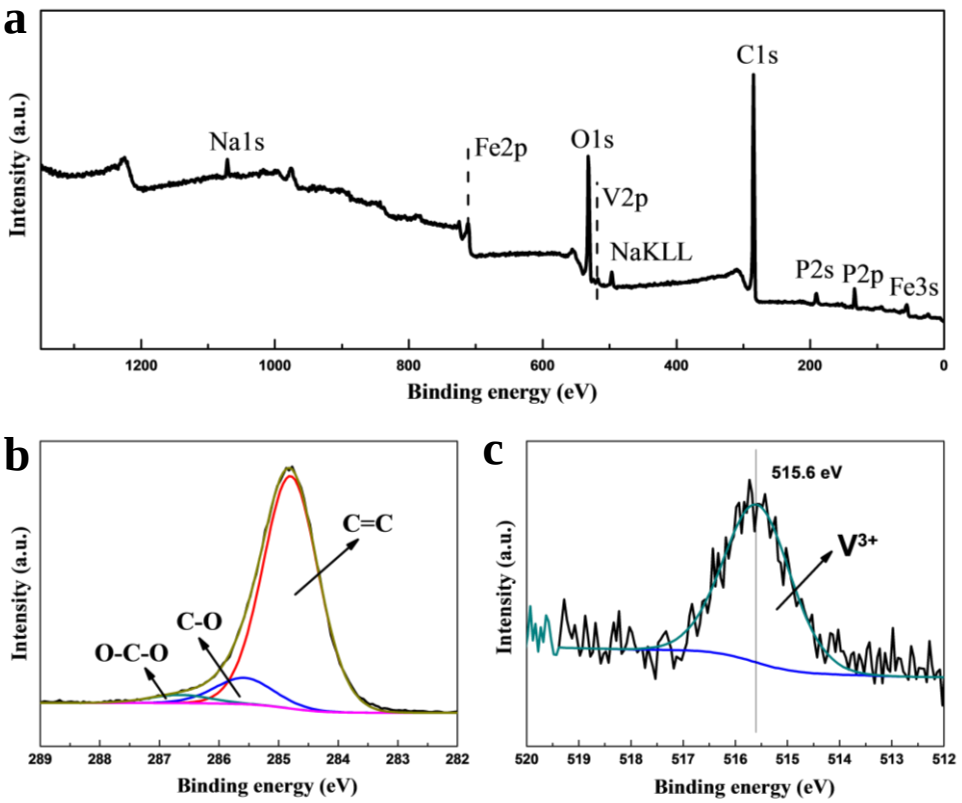

Fig.4 XPS of LFP@NVP@C: (a) XPS survey, (b) High resolution of C1s curve, (c) High resolution of V2p curve.

RARE METALS
www.editorialmanager.com/rmet

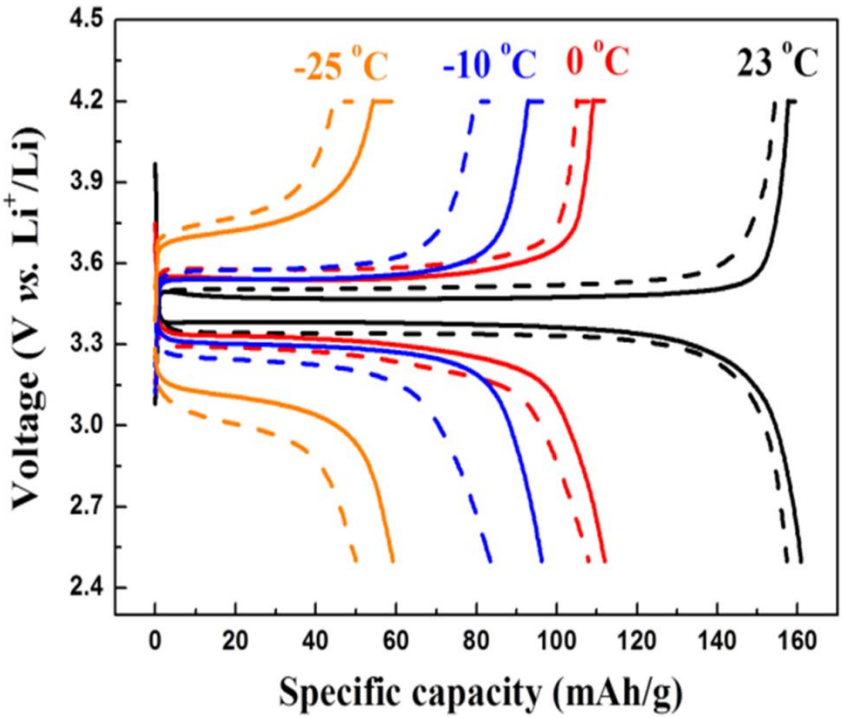

Fig.5 Electrochemical tests of LFP@NVP@C (solid line) and LFP@C (dash line) at various temperatures: Charge/discharge profiles with 0.5 *C*.

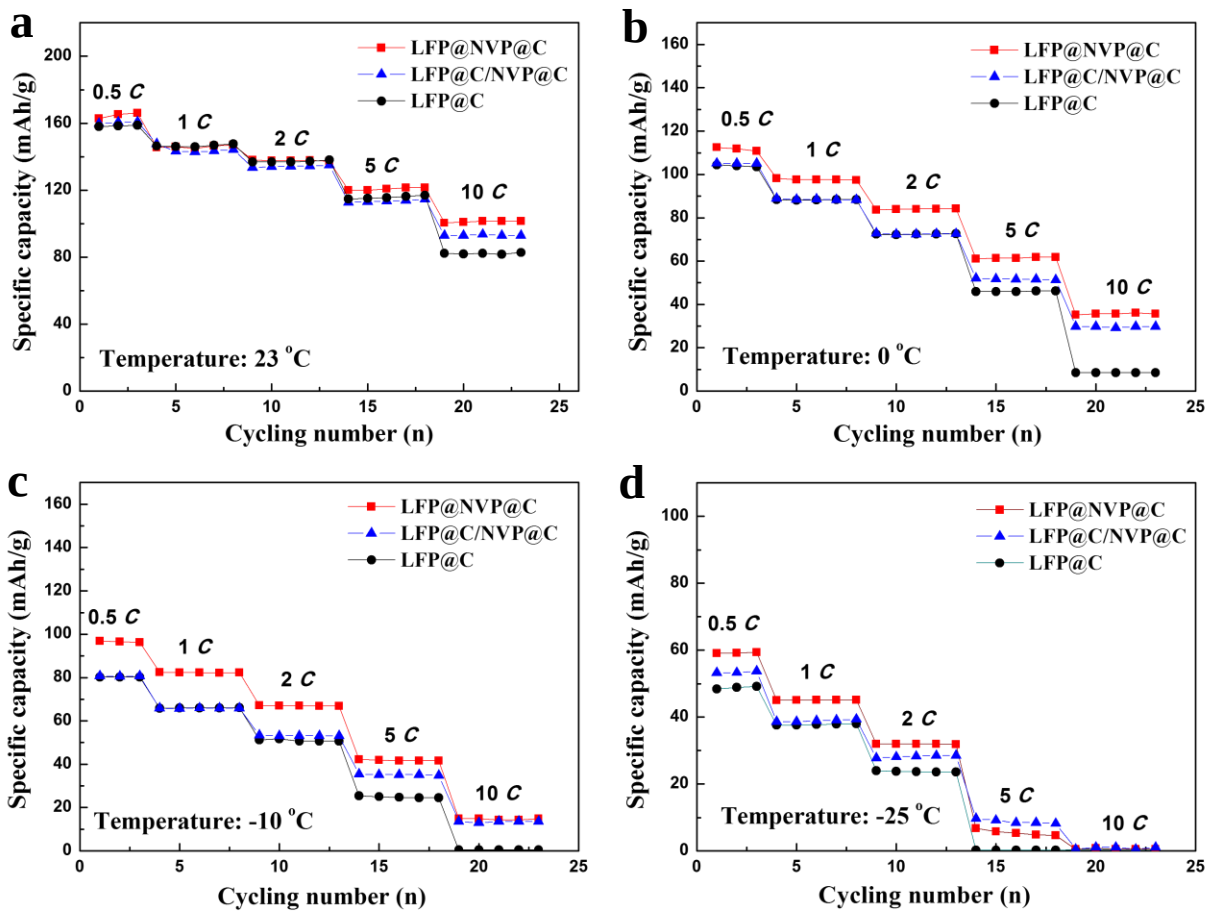

Fig.6 Rate performance of the LFP@NVP@C, LFP@C and LFP@C/NVP@C at different temperatures: (a) 23 ºC; (b) 0 ºC; (c)-10 ºC; (d)-25 ºC.

RARE METALS
www.editorialmanager.com/rmet

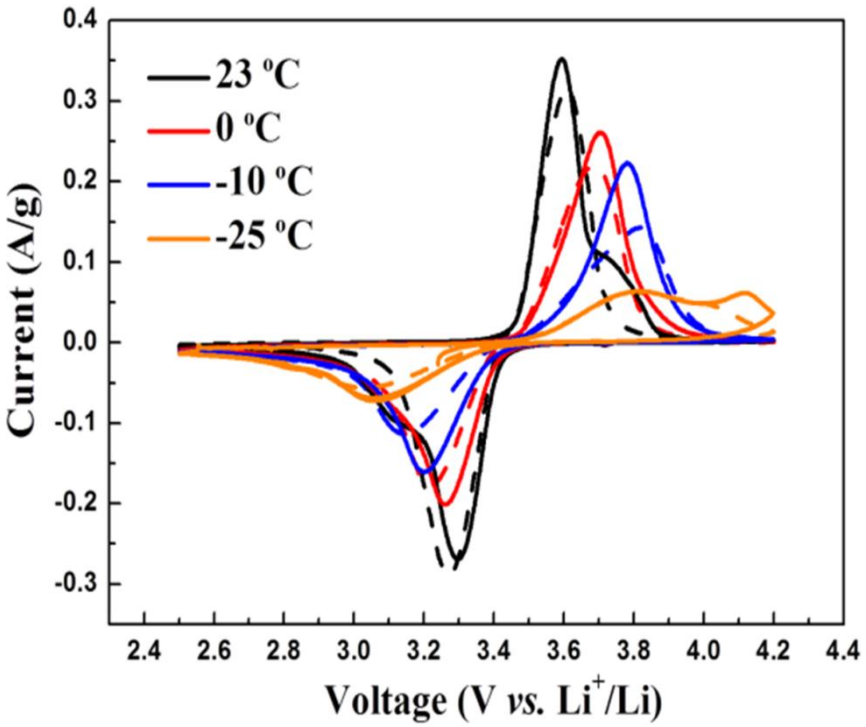

Fig.7 CV measurements of LFP@NVP@C (solid line) and LFP@C (dash line) electrode with the scanning rate of 0.1 mV·s^{-1}.

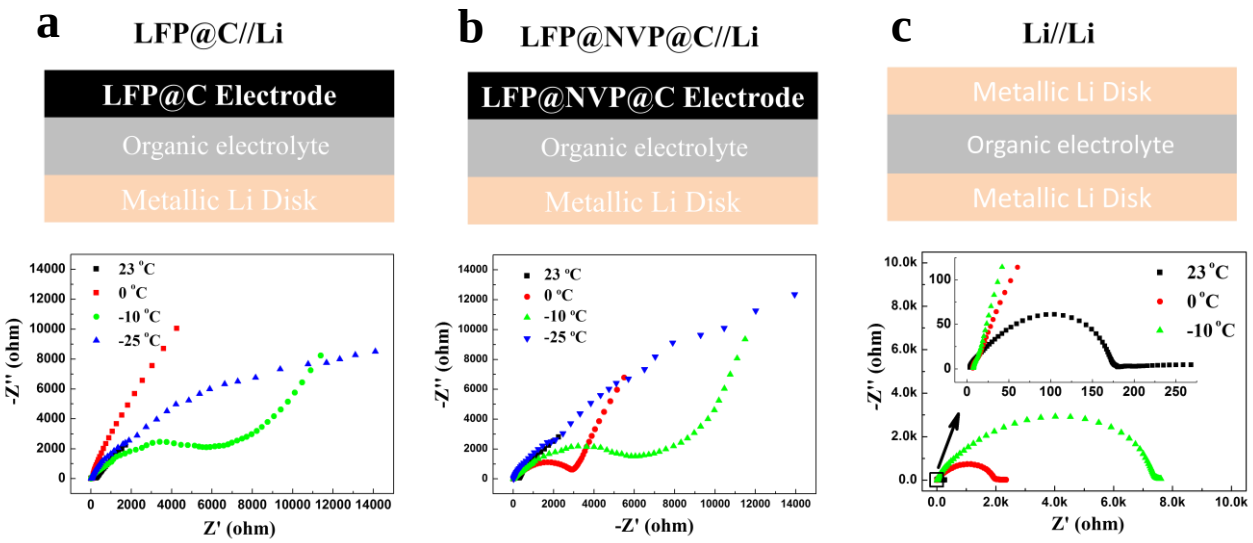

Fig.8 EIS characterizations at different temperatures: (a) Cell structure and resultant EIS curves of the LFP@C; (b) Cell structure and resultant EIS curves of the LFP@NVP@C; (c) Cell structure and resultant EIS curves of symmetric Li disks.

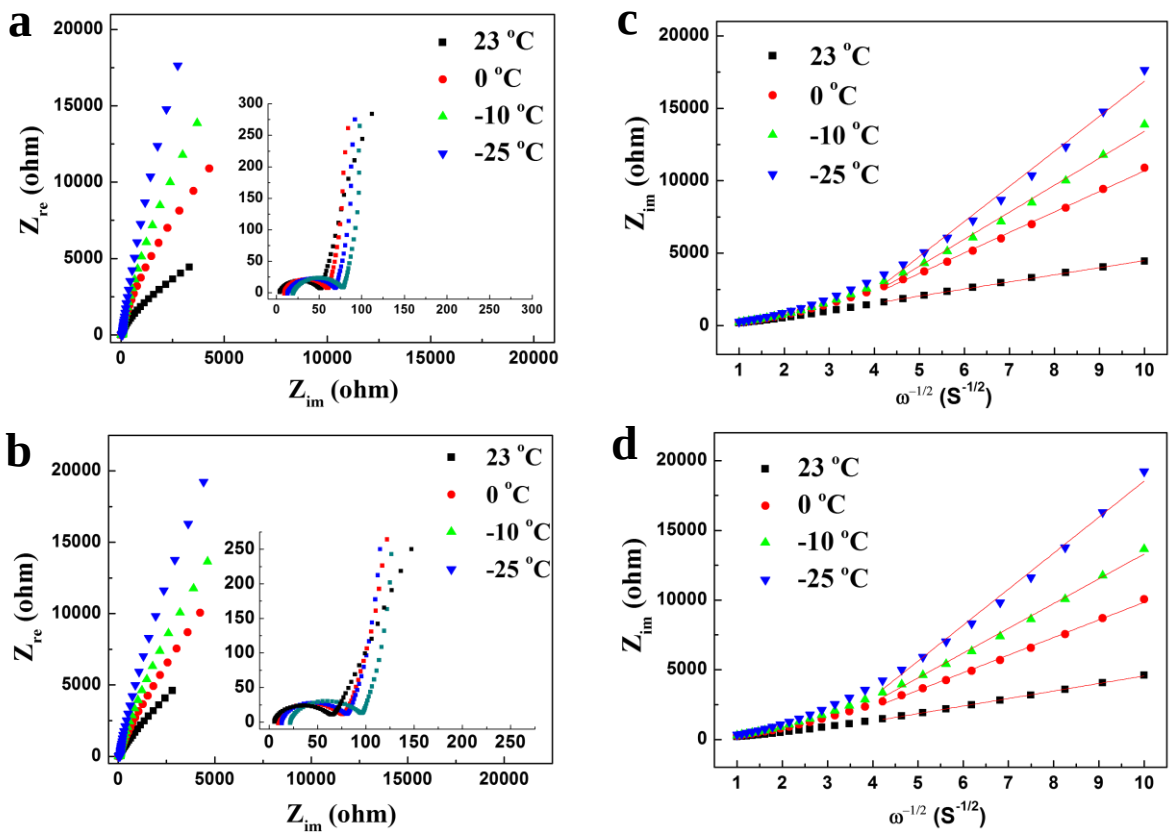

Fig.9 EIS characterizations of symmetrical electrode at different temperatures: EIS curves of the (a) LFP@NVP@C and (b) LFP@C; The fitting curves of $-Z_{Im}$ and $\omega^{-1/2}$ at low frequency region for (c) LFP@NVP@C and (d) LFP@C.